Earth and Planetary Science Letters 300 (2010) 351–358

Contents lists available at ScienceDirect

Earth and Planetary Science Letters

journal homepage: www.elsevier.com/locate/epsl

Implications of initial conditions and ice–ocean coupling for grounding-line evolution

Byron R. Parizek [a,*], Ryan T. Walker [b,1]

[a] Mathematics and Geosciences, 181 Smeal Building, Penn State DuBois, College Place, DuBois, PA 15801, United States
[b] Department of Geosciences and Earth and Environmental Systems Institute, 534 Deike Building, The Pennsylvania State University, University Park, PA 16802, United States

ARTICLE INFO

Article history:
Received 13 March 2010
Received in revised form 11 October 2010
Accepted 12 October 2010
Available online 13 November 2010

Editor: P. DeMenocal

Keywords:
ice stream
ice shelf
ocean
glacier dynamics

ABSTRACT

Ice-sheet grounding lines are sensitive to initial conditions and to small perturbations in boundary conditions, based on new model results coupling ocean and ice flow. To study ice–ocean dynamics near ice-stream grounding lines, we couple an ocean-plume model that simulates ice-shelf basal melting with a two-dimensional, isothermal model of ice-stream and ice-shelf flow. The notable results of the coupled model experiments are to reveal grounding-line migration sensitivities to i) specific aspects of modeling-derived and history-dependent initial conditions, ii) to the overall melt magnitude, and iii) to a positive feedback between focused melting and local slopes of basal ice that is eventually stabilized by buttressing for lengthening ice shelves. These interactions can lead to multiple steady states for ice flow over a bed that shallows in the along-flow direction and have an important bearing on the effects of bedrock bumps.

When in the vicinity of bedrock highs, grounding lines tend to rapidly advance or retreat towards the basal asperity. A significant delay or cessation of (de)glaciation occurs once the grounding line reaches the leeward side of the bedrock crest. However, while bedrock bumps can offer stability in the grounding zone, minor changes in ocean conditions can easily offset their effect through basal melting feedbacks.

1. Introduction

While the vast, slowly-deforming interior regions of the Antarctic and Greenland Ice Sheets are presently receiving increased snowfall, the lower elevations of many ice streams and outlet glaciers are experiencing dramatic adjustments due to changes in ice dynamics and/or surface mass balance (Rignot et al., 2008a,b). Where floating ice shelves buttress inland ice-stream flow, forcings that alter the geometry of the ice shelf can potentially lead to a response well upstream in the snow catchment area for the stream–shelf system, thereby influencing the mass balance for the entire outlet basin (e.g. Dupont and Alley, 2005, 2006; Hulbe et al., 2004; Joughin et al., 2004; Payne et al., 2004; Rignot et al., 2008a,b; Scambos et al., 2004; Thomas et al., 2004; Vieli and Payne, 2005).

Observations and theory suggest that ice shelves are very sensitive to changes in their boundary conditions, regardless of the mechanism that ultimately led to the change (Holland et al., 2008; Payne et al., 2007; Scambos et al., 2000, 2003; Sergienko and MacAyeal, 2005; Van den Broeke, 2005). Although immediate impacts on global sea-level of recent shelf disintegration are relatively minor to date, dynamic feedbacks can potentially lead to significant and prolonged changes, especially with sustained forcing (e.g., Holt et al., 2006; Howat et al., 2005; Parizek and Alley, 2004; Parizek et al., 2010; Solomon et al., 2007).

Furthermore, numerous studies have found that in a marine setting (the base of the ice is below sea-level) discrete, stable equilibria exist only on downsloping beds (the bed deepens in the down-glacier direction; e.g., Durand et al., 2009; Goldberg et al., 2009; Schoof, 2007a; Weertman, 1974). Along an upsloping bed, theory indicates that the forcing does not need to be sustained to produce significant changes in the ice mass. The so-called marine instability predicts that the grounding-line (location where a grounded ice stream or outlet glacier transitions into a floating ice shelf or ice tongue) will advance or retreat unstably if perturbed, because of the dependence of ice flux across the grounding-line on grounding-line ice thickness for a freely-floating ice shelf (e.g., Schoof, 2007a,b; Thomas, 1977; Thomas and Bentley, 1978; Weertman, 1974). In addition, Schoof's (2007a,b) analyses indicate that this flux-thickness relationship is a result of the dependence of ice flux on longitudinal stress. Because ice-shelf buttressing changes the stress regime at the grounding-line, this dependence implies that buttressing can potentially alter the temporal evolution of the outlet system as well as the above stability characteristics (Schoof, 2007a). Indeed, Dupont and Alley (2005) and Goldberg et al. (2009) have found that ice flow

* Corresponding author.
E-mail address: parizek@psu.edu (B.R. Parizek).
[1] Now at the Department of Mathematics and Computer Science, Bemidji State University, Bemidji, MN 56601, United States.

0012-821X/$ – see front matter © 2010 Elsevier B.V. All rights reserved.
doi:10.1016/j.epsl.2010.10.016

through narrow channels with weak beds can lead to sufficient lateral shearing to generate stable equilibria on upsloping beds. Goldberg et al. (2009) further suggest that ice rises can effectively narrow regional flow channels and thereby offer stability to wide outlet systems as well.

In this study, we extend the above theoretical work by investigating the dynamic response of an ice shelf and its buttressed ice stream to different ocean conditions. We test the effect of basal melting on the stability characteristics of narrow outlet systems and address whether the initial state of the ice–ocean system is important or if knowledge of the forcing and boundary conditions are sufficient for predicting grounding-line evolution and catchment response. Answering these fundamental questions can improve our understanding of the diversity in regional responses and inform future assessments by evaluating the impact of history dependence and model initialization on system dynamics. In order to isolate the effects of ocean circulation on ice shelves (and, through buttressing variability, on ice-stream flow and grounding-line motion), we perform ice-shelf perturbation experiments using reduced-dimensional modeling of a coupled ice stream–ice shelf–ocean system.

2. Methods

2.1. Coupled model

2.1.1. Ice flow

Ice flow is simulated using the Parizek et al. (2010) two-dimensional, isothermal finite element model. We assume power law rheology for ice (Eqs. (1)–(2); Budd and Jacka, 1989; Glen, 1955), a width-averaged, horizontal momentum balance for sheet, stream, and shelf flow (Eq. (3); MacAyeal, 1989; Pattyn, 2002; Parizek et al., 2010, and the flux form of the continuity equation for mass balance (Eq. (4)):

$$\sigma'_{ij} = 2\nu\dot{\varepsilon}_{ij}$$
$$\nu \equiv \frac{B}{2}\dot{\varepsilon}_*^{\frac{(1-n)}{n}} \tag{1}$$

$$= \frac{B}{2}\left\{\left(\frac{\partial u}{\partial x}\right)^2 + \frac{1}{4}\left(\frac{\partial u}{\partial z}\right)^2\right\}^{\frac{(1-n)}{2n}} \tag{2}$$

$$\frac{\partial}{\partial x}\left(4\nu\frac{\partial u}{\partial x}\right) + \frac{\partial}{\partial z}\left(\nu\frac{\partial u}{\partial z}\right) = \rho g\frac{\partial(s-z)}{\partial x} + \frac{2}{\beta}\tau_s \tag{3}$$

$$\frac{\partial h}{\partial t} = -\frac{\partial\left(h\bar{u}\right)}{\partial x} - m \tag{4}$$

where σ'_{ij} and $\dot{\varepsilon}_{ij}$ are the deviatoric stress and strain-rate components of their respective tensors, ν is the effective viscosity, B is the ice-hardness parameter, $\dot{\varepsilon}_*$ is the effective strain-rate, n is the flow-law exponent, u is the horizontal velocity ($\bar{u}$ for its depth-averaged value), ρ is the density of ice, g is the acceleration due to gravity, s is the ice-surface elevation, β is the flowband width, τ_s is the lateral drag, h is the ice thickness ($h = s - b$, where b is the basal elevation of the ice), and m is the ice-equivalent basal melting rate for the ice shelf that is calculated by the ocean model. Lateral drag is parameterized as a boundary-layer phenomenon dominated by side shear within ice (e.g., Dupont and Alley, 2005; Parizek et al., 2010). By assuming side drag does not induce significant lateral gradients of horizontal velocity outside a narrow shear zone, we are treating it as a horizontal body force balanced by longitudinal and vertical deviatoric stress gradients within the main channel. Favorable comparisons between simulations with parameterized versus unparameterized lateral drag on similar shelf geometries (e.g., Dupont, 2009; Goldberg et al., 2009) support this simplifying assumption.

As boundary conditions for the momentum balance Eq. (3), we specify dynamic conditions at the surface (stress free) and bed (basal drag and/or normal stress):

$$\left(4\nu\frac{\partial u(z)}{\partial x} - \rho g(s-z)\right)\frac{\partial z}{\partial x} - \nu\frac{\partial u(z)}{\partial z} = R$$
$$R = \begin{cases} 0 & \text{at the surface} \\ -\tau_b - \rho g h\dfrac{\partial b}{\partial x} & \text{at the bed, for all grounded ice} \\ \rho_{sw} g b\dfrac{\partial b}{\partial x} & \text{at the bed, for all floating ice,} \end{cases} \tag{5}$$

as well as at the vertical ice front (stress free or hydrostatic):

$$4\nu\frac{\partial u(x)}{\partial x} - \rho g(s-z) = \begin{cases} 0 & z \geq 0 \\ \rho_{sw} g z & b < z < 0, \end{cases} \tag{6}$$

where ρ_{sw} is the density of seawater. In grounded regions, we assume basal drag results from deformation of a linear viscous substrate, such that $\tau_b = B_b u(b)$ (where B_b is the basal friction coefficient; see Table 1 for a list of parameter values). The dynamic conditions specified in Eq. (6) are either applied at $x = x_{if}$, when the ice front is within the domain, or at the terminal end, $x = L$, otherwise (where x_{if} is the ice front position and L is the length of the flowline). Beyond the domain ($x > L$), we assume that the ice is freely-floating (i.e., it does not experience ephemeral grounding or lateral drag) and therefore provides no additional buttressing to the stream–shelf system. At the upstream end of the domain ($x = 0$), we specify a time-dependent Dirichlet boundary condition, $u(0,t) = q_o/h(0,t)$, determined from the ratio of a prescribed upstream flux and an evolving ice thickness.

At the upstream and downstream ends of the flowline, constant flux (q_o) and free-radiation boundary conditions are applied, respectively, to Eq. (4). Regions of the ice shelf that are less than 10 m thick are calved. If this causes the ice front to retreat into the domain channel ($x_{if} < L$), the free-radiation condition is no longer applied, as the position of the ice front evolves based on mass balance considerations. While we would expect iceberg formation well before the shelf reached this minimum threshold, Parizek et al. (2010) demonstrated that selecting a larger value, on the order of 100 m, induces modeling-imposed hysteresis by limiting glaciation. Parizek et al. (2010) also illustrated that retaining a thin shelf front in the model provides minimal additional buttressing and therefore negligible dynamic influence on ice shelf–ice stream flow.

Along-flow nodal spacing is 1 km for the mass balance computation and adaptively refined for the momentum–balance calculations, with high resolution (100 m) in the grounding zone to minimize numerical artifacts that affect grounding-line migration (e.g., Durand et al., 2009; Goldberg et al., 2009; Parizek et al., 2010; Vieli and Payne, 2005). Simulations producing multiple steady states were tested at 2 km, 1 km, and 0.5 km nodal spacings, with adaptive refinement

Table 1
Model parameters.

Notation	Description	Value
α	Bed slope	1.00×10^{-3}
β	Flowband width	40 km
B	Ice-hardness parameter	1.27×10^{8} Pa s$^{1/3}$
B_b	Basal friction coefficient	2.0×10^{9} Pa m^{-1} s
B_s	Side-friction coefficient	2.8×10^{6} Pa m$^{-1/3}$ s$^{1/3}$
g	Gravitational acceleration	9.81 m s^{-2}
L	Domain length	150 km
n	Flow-law exponent for ice	3
q_o	Upstream flux	1.6×10^{3} m^3 s^{-1}
ρ	Density of ice	917 kg m^{-3}
ρ_{sw}	Density of sea water	1028 kg m^{-3}

down to 200 m, 100 m, and 50 m, respectively, to ensure that our results are due to ice–ocean feedbacks rather than numerics. Furthermore, for all experiments, we employ sub-gridscale linear interpolation of the grounding-line position based on the flotation criterion to enable partial element scaling of the basal drag when calculating ice velocities (e.g., Pattyn et al., 2006; see Parizek et al. (2010) for model validation).

2.1.2. Ocean plume

The shape of the ice-shelf cavity evolves with the ice flow and impacts the ocean-plume thermodynamics. The plume model is a slightly modified version of the Jenkins (1991) model, consisting of diagnostic equations for continuity (Eq. (7)), momentum (Eq. (8)), and heat and salt conservation (Eqs. (9)–(10)) in terms of plume velocity (U), thickness (D), temperature (T), and salinity (S).

$$\frac{d}{dx}(UD) = e + m \tag{7}$$

$$\frac{d}{dx}\left(U^2 D\right) = -\epsilon D \Delta\rho g \sin\theta - kU^2 \tag{8}$$

$$\frac{d}{dx}(TUD) = T_w e + T_b m + (T_b - T)\gamma_T \tag{9}$$

$$\frac{d}{dx}(SUD) = S_w e + S_b m + (S_b - S)\gamma_S \tag{10}$$

Ambient water properties T_w and S_w are assumed to be functions of depth, with a slight linear stratification imposed to ensure water-column stability. The rate of entrainment e of this underlying water into the plume is given by the parameterization of Stigebrandt (1987). Water properties at the shelf base (T_b and S_b), the basal melt rate (m), and the velocity-dependent exchange coefficients (γ_T and γ_S) are calculated as in Holland and Jenkins (1999).

We note that the momentum equation for the plume Eq. (8) is a balance of buoyancy and drag, where ϵ is a geostrophic parameter and k is a frictional drag coefficient. Borrowing from global meridional overturning circulation models (Drbohlav and Jin, 1998; Wright and Stocker, 1991), we parameterize the Coriolis term from the full three-dimensional momentum equation as a function of the along-flow pressure gradient. The result is the parameter $\epsilon \in [0,1]$, where $\epsilon = 0$ for geostrophic balance and $\epsilon = 1$ for negligible transverse flow. This method accounts for the Coriolis term by limiting plume velocities, but cannot capture deflection of the plume due to the lack of a transverse dimension in the model. However, because we are only considering relatively narrow ice shelves with our flowline model, we do not expect this limitation to have any major effect on the process studies we present.

The ice shelf must have a positive basal slope in the initiation region near the grounding zone in order to develop a buoyant plume with a positive velocity. At times, when the grounding-line is on the leeward side of the bedrock bump, a negative basal slope can develop. In this case, we start the plume model a few kilometers downstream. (Furthermore, if the plume attains neutral buoyancy elsewhere, it separates from the ice-shelf base and the plume model no longer applies; however, this condition does not occur in these scenarios.) The basal slope of the ice shelf, θ, plays an important role in driving faster flow under steeper regions of the shelf base. Because the turbulent exchange coefficients depend on plume velocity, melting is greatest in areas of high basal slope (Little et al., 2009). When the ice-shelf profile is allowed to evolve in response to melting, the result is a positive feedback that tends to increase the slope of steep regions, until balanced by horizontal advection of ice (Walker and Holland, 2007).

The use of a steady-state plume model (7–10) is justified here, because the time it takes for the ice-shelf cavity to evolve sufficiently to impact the melt rates is longer than the few years that would be required for the ocean to reach a new steady state. To ensure the melt rates reflect the cavity shape, we call the plume model either every five simulated years or as soon as the grounding-line has moved more than two kilometers, whichever comes first.

2.2. Simulations

Each simulation spans 1500 yr. The flowline domain consists of a L = 150 km long, parallel-sided channel of width β = 40 km (Fig. 1). The bed slopes upward and includes a ~16 km long, 50 m high bedrock bump centered at 50 km along the flowline (Fig. 2a). In choosing an upsloping bed, we focus on dynamic variability applicable to marine ice sheets (e.g., Schoof, 2007a,b; Thomas, 1977; Thomas and Bentley, 1978; Weertman, 1974).

Alley et al. (2007) found that a bedrock bump/sediment wedge similar in size to the one that we include in our domain can provide grounding-line stability through several meters of sea-level rise or a few percent reduction in buttressing. Analyses of satellite imagery and local ice-penetrating radar data indicate that rapid flow across relatively static grounding lines often corresponds to an inflection in surface slope and that this break in surface slope on Whillans Ice Stream in West Antarctica is caused by a change in bed slope (Anandakrishnan et al., 2007; Fricker et al., 2009; Horgan and Anandakrishnan, 2006). In addition, characterization of the radar echo implies that the basal high is likely composed of sediment

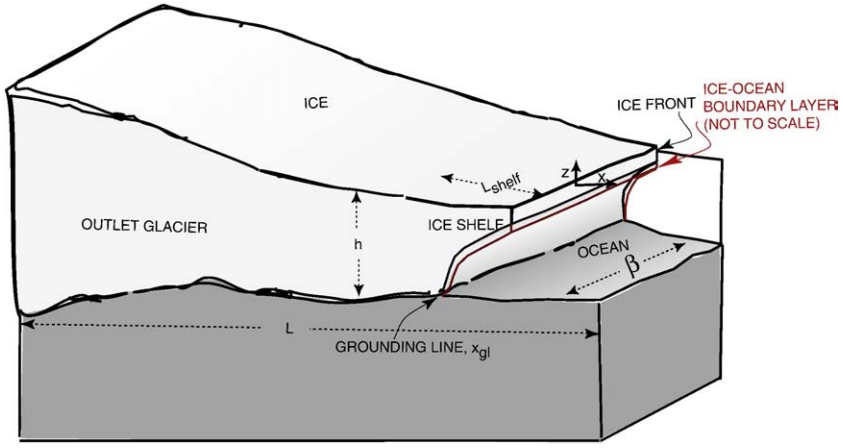

Fig. 1. Schematic diagram of the model domain. In the studies presented here, the ice–ocean boundary-layer thickens along-flow to a maximum thickness of ≈15–35 m.

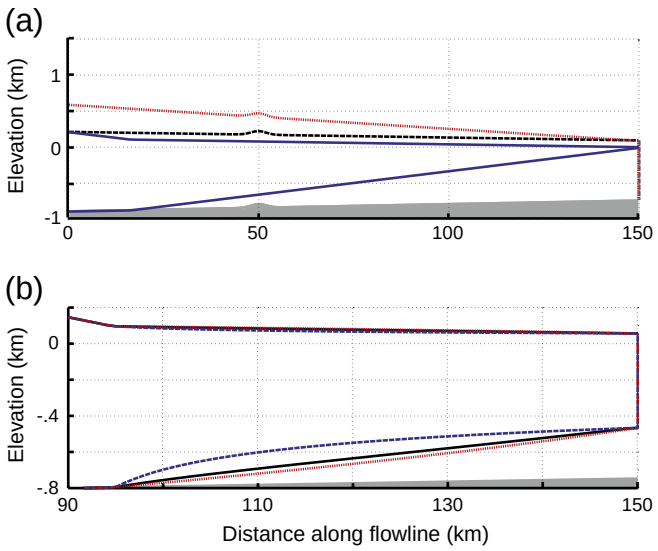

Fig. 2. Initial conditions for the ice stream–ice shelf profile. (a) The dashed black line represents an ice-thickness profile that is grounded, yet close to flotation, across the entire domain. The dotted red profile has an upstream ice thickness that is similar to the steady-state values and a downstream thickness equivalent to the dashed black initial condition. The blue profile represents partial grounding (note that the grounding-line is behind the bedrock bump/sediment wedge). (b) Concavity changes implemented prior to ocean coupling in the second set of runs. The ice-shelf base resulting from the steady-state profile without ocean coupling (black) is either carved out (concave, dashed blue) or expanded out (convex, dotted red). The axes have been rescaled to highlight the ice-shelf profiles.

(Anandakrishnan et al., 2007). Regardless of composition, numerous theoretical studies have found that grounding lines of fast flowing ice streams and outlet glaciers will tend to stabilize on basal topographic highs (e.g., Alley et al., 2007; Durand et al., 2009; Schoof, 2007a). Here we focus on ice–ocean interactions to further test the effect of basal morphology on grounding-line motion and to quantify the "fairly subtle perturbation in water temperature" (Alley et al., 2007) required to destabilize the grounding line from low-amplitude bedrock highs.

In order to assess system sensitivity to initial and boundary conditions, we perform experiments that vary the initial ice profile and state of the ocean. The three sets of experiments focus on the effects of i) ambient ocean conditions in determining whether the system responds linearly or non-linearly to the state of the ocean, ii) ice-shelf cavity shape in determining whether ice–ocean feedbacks are stable or unstable, and iii) initial conditions in determining whether the impact of ice–ocean coupling on shelf shape, and therefore on buttressing, generates single or multiple equilibria on an upsloping bed.

We initialize our model runs with one of three ice profiles: a) a grounded ice stream that is tapered from an upstream thickness that is 100 m above flotation down to the flotation thickness at $x=L$, b) a thicker ice stream that is tapered from an upstream thickness of 1480 m (480 m above flotation) down to the flotation thickness at $x=L$, or c) a thin ice stream in the first ~16 km and an ice shelf that covers the remaining ~134 km of the domain (dashed black, dotted red, and solid blue profiles in Fig. 2a, respectively).

In the first set of experiments, these ice profiles are run to an initial steady state without ocean coupling (i.e., there is no ice-shelf basal melting, so the only source and sink of ice are the upstream influx and downstream free-radiation conditions, respectively) to establish that these arbitrary initial conditions lead to a single steady state (dashed profiles in Fig. 3) for the shelf–stream system. Steady state is reached at t_{SS}, after 500 consecutive years during which no year has a change in ice volume as large as 0.01%. Subsequently, for $t_{SS}<t\leq 1500$ yr, the ocean-plume model is coupled to the ice stream–ice shelf model within the evolving ice-shelf cavity. Five different ambient ocean conditions are tested to determine system response to water-mass characteristics. We start with an ocean-surface temperature of $T_w(z=0)=-1.9\,^{\circ}\mathrm{C}$ (indicative of cold High Salinity Shelf Water (HSSW) resulting from sea–ice formation) and then warm the ocean for the remaining four simulations to include $T_w(0)=-1.5\,^{\circ}\mathrm{C}$, $-1.25\,^{\circ}\mathrm{C}$, $-1\,^{\circ}\mathrm{C}$, and $-0.75\,^{\circ}\mathrm{C}$. (With the chosen boundary conditions in these simulations, the grounding line retreats off the domain under the $T_w(0)=-0.75\,^{\circ}\mathrm{C}$ ocean forcing. Therefore, the warm, $T_w(0)\approx 1\,^{\circ}\mathrm{C}$, Circumpolar Deep Water (CDW) end-member case is not tested here, as it would only change the temporal evolution of the results.)

In our second set of runs, we test system sensitivity to changes in cavity shape by artificially altering the steady-state ice-shelf-bottom geometry just prior to activating the $T_w(0)=-1.25\,^{\circ}\mathrm{C}$, $-1\,^{\circ}\mathrm{C}$, and $-0.75\,^{\circ}\mathrm{C}$ ocean-forcing scenarios (dashed blue and dotted red profiles in Fig. 2b). In removing (adding) ice to make the base of the shelf more concave (convex), we are altering the buoyancy-driven plume flow, and hence the magnitude and distribution of basal melt. Because the feedback in a coupled ice–ocean model may tend to increase these differences in melt profiles (Walker and Holland, 2007) and spatial distribution of melting has been found to affect grounding-line migration (Walker et al., 2008), it is possible that the dynamic response could amplify differences in initial conditions and produce multiple steady states or a runaway positive feedback.

Our third and final set of experiments includes ocean coupling from the start of the simulations, $t=0$ yr, with either $T_w(0)=-1.25\,^{\circ}\mathrm{C}$ or $-1\,^{\circ}\mathrm{C}$ surface-water conditions (these ambient temperatures were chosen based on the results from the previous experiments). If a single equilibrium exists for each ambient ocean condition, then the choice of initial conditions should not alter the steady-state results from our first set of experiments. If, on the other hand, the interactions between the ocean plume and the ice sufficiently alter the flow and shape of the ice shelf and, therefore, ice-shelf buttressing, different steady-state profiles might arise.

3. Results

In the absence of ocean forcing ($m=0$ m/yr), all initial profiles we tested evolve to a discrete steady-state profile for the ice stream–ice shelf system (shown dashed in all five panels of Fig. 3). While the thin versus thick, fully grounded initial conditions (dashed black and dotted red in Fig. 2a, respectively) lead to two distinct steady states at the 1-km grid resolution (solid black and solid red curves around 500 yr in Fig. 5a, respectively), the profiles converge as we reduce grid spacing from 2 km, to 1 km, and finally down to 0.5 km. This suggests that the offset is due to numerics rather than two distinct equilibria for the system (see Appendix A in Parizek et al., 2010).

On the 1-km grid with mesh refinement down to 100 m, steady-state ice thickness and velocity at the upstream (downstream) end of the domain are approximately 1564 m (523 m) and 807 m/yr (2419 m/yr), respectively. The grounding-line is located at 94.7 km (44.7 km beyond the bedrock bump). Therefore, given our domain and boundary conditions, the single, unforced steady-state grounding-line position arising from the various initial conditions is not a consequence of the stabilizing effects of the bedrock high. However, as expected, the evolution of the system is highly dependent on the artificial initial conditions (cf. the first 250–350 years of the solid black, solid red, and dot–dashed cyan curves in Fig. 5; see Table 2 for line-type designations for the various experiments). The differences among these paths to steady state will become important when oceanic forcing is applied from the beginning of the simulations (see Section 3.3).

When the initial condition is a fully grounded ice stream that is much thinner than at steady state, the deglaciation overshoots the steady-state grounding-line (e.g., solid black curves in Fig. 5, during

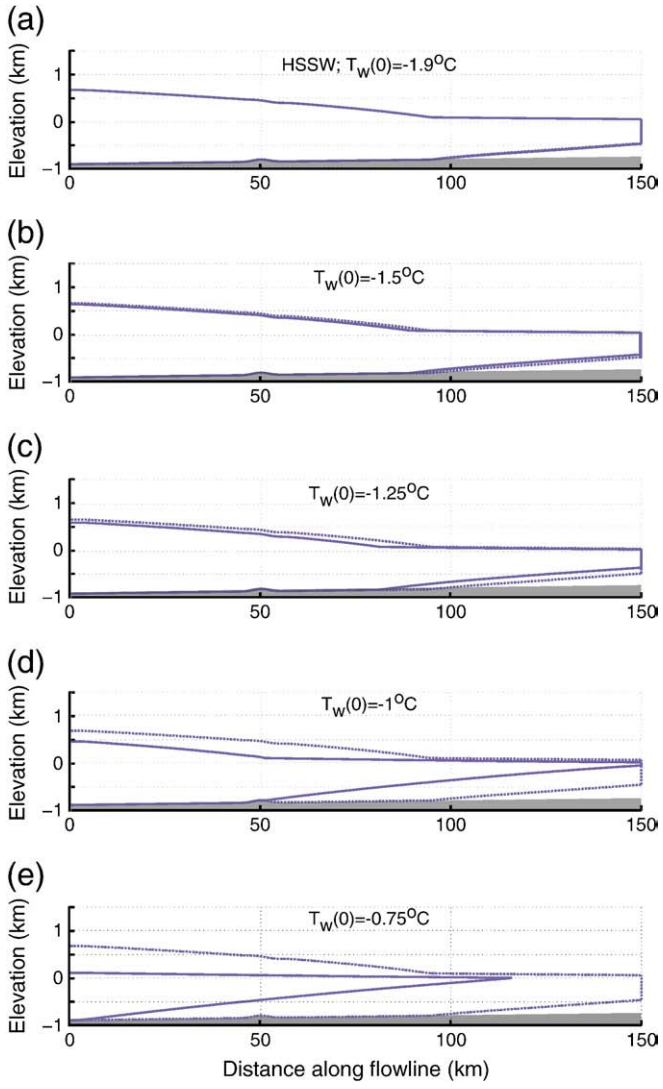

Fig. 3. Steady-state profiles reached prior to (dashed lines; panels a–e) and after (solid lines; panels a–d) ocean coupling. The panels represent coupled runs with progressively warmer ocean conditions. The ocean-surface temperatures are (a) −1.9 °C, indicative of cold High Salinity Shelf Water (HSSW), (b) −1.5 °C, (c) −1.25 °C, (d) −1.0 °C, and (e) −0.75 °C, respectively. The solid profile in (e) is a snapshot just prior to the ice stream decoupling from the bed across the entire domain.

the first few decades; cf., the grounding-line position depicted by the solid red curve for the thicker initial condition approaches steady state exponentially). An overshoot will exist as long as the residence time of through-going ice is long enough (e.g., upstream flux is low enough and/or the basal or side-friction are high enough) to delay ice transport to the retreating grounding zone. The ice then advances to its steady-state grounding-line position at 94.7 km by about 250 simulated years (Fig. 5).

With the partially grounded initial condition, an initially rapid advance to and an acceleration up the upstream side of the bedrock high is followed by a ~40-year period of grounding-line stasis as the bump resists further glaciation (e.g., dot–dashed cyan profiles in Fig. 5; Durand et al., 2009; Schoof, 2007a). The acceleration along the upstream side is due to the along-flow reduction in grounding-line flotation thickness. This increases drag between the ice and basal wedge, leading to ice-stream thickening in the grounding zone region (Alley et al., 2007). The grounding-line continues its swift advance only after the ice stream thickens sufficiently to ground along the entire leeward side of the bedrock high.

3.1. Set one: Ambient ocean forcing

The behavior of the ice–ocean system depends non-linearly on ambient water conditions (as shown by the final steady-state profiles in Fig. 3). In all five ice-shelf cavities depicted here, the maximum melt rates are focused near the grounding line and vary exponentially with surface-water temperature ($m_{max} = 1.6, 4.8, 8.3, 13.6, 20.5$ m/yr), with indirect contributions arising from changing shelf geometry and grounding-line depth in the coupled simulations. The ocean has only a relatively minor impact on the ice due to the minimal loss of ice-shelf buttressing through 0.65 °C warming of HSSW ($\Delta x_{gl} \approx 14$ km, cf. Fig. 3a,c). However, an additional warming of 0.25 °C results in another 30 km of deglaciation (cf. Fig. 3c,d; final steady-state grounding-line positions depicted by solid black or dot–dashed cyan curves in Fig. 5a,c). Furthermore, the ice-stream retreat for the $T_w(0) = -1.0$ °C forcing ends only when the grounding-line reaches the stabilizing bedrock bump (coming to rest on the leeward side at $x_{gl} = 51$ km, Fig. 3d; cf., continued deglaciation in the absence of the 50-m high obstacle as depicted in Fig. 5c), with slightly warmer ocean conditions leading to complete deglaciation of the model domain (e.g., Fig. 3e).

Under ocean scenarios that cause deglaciation to and/or past the bedrock bump, the rate of deglaciation initially accelerates once the grounding-line approaches the leeward side of the mound ($x_{gl} \approx 58$ km; under the $T_w(0) = -1.0$ °C forcing, curves start to become roughly horizontal in Fig. 5c–d). The rapid retreat continues until $x_{gl} \approx 52$ km, at which point the stabilizing effect of the wedge becomes prominent. Shallowing of the bed during ice-stream retreat on the leeward side should (and eventually does) offer stability. However, this stability is temporarily offset as the grounding-line retreats towards the region where the ice-surface flattens a few ice thicknesses down-glacier of the bump's apex. The ice thickness above flotation does not increase as much when moving upstream through this region. This leads to the rapid deglaciation.

During complete deglaciation of the model domain, this rapid 6-km retreat is followed by a ~60 year delay in deglaciation as the grounding-line slowly works its way up a 3-km stretch (starting at $x_{gl} \approx 52$ km) along the leeward side and over the crest of the topographic high. Once the grounding-line pulls back to $x_{gl} \approx 49$ km, retreat rates accelerate once again as deglaciation continues down the upstream side of the basal bump. This second episode of accelerated retreat is the result of a temporary enhancement of the marine instability associated with the increased basal slope. For the partially grounded initial condition, the 20-year difference between the delay in ice advance during model spin-up (40 years) versus retreat (60 years) over the basal asperity largely results from forcing (ocean off versus on, respectively) and volume–above flotation differences, although hysteresis arising from advance and retreat dynamics is also present (Parizek et al., 2010).

3.2. Set two: Ice-shelf cavity shape

Changing the concavity of the shelf bottom as we activate ice–ocean coupling alters the timing of retreat but not the final grounding-line position. When the ocean is activated, the peak melting rates are in the ~8–18 m/yr range, with ambient ocean conditions and shelf geometry largely controlling the maximum value and the location of peak melt, respectively (Fig. 4). Even with the positive feedback between basal slope and melt rates, these values are not high enough to sustain the shelf geometry perturbations due to the relatively large ice fluxes in our simulations. With retreat in a marine setting, ice flux increases at the grounding-line unless the ice shelf provides enough buttressing to reduce the local longitudinal stress (Dupont and Alley, 2005; Goldberg et al., 2009; Schoof, 2007a,b). When the ocean is activated, the longitudinal deviatoric stress in the grounding zone is simply too large and the resulting ice flux overpowers the ability of the ocean forcing to maintain or amplify the artificially altered cavity

Table 2
Simulation definitions in relation to the results shown in Fig. 5.

Simulations	Description	$T_w(0)$ (°C)	Grounding-line history in Fig. 5
Ambient ocean conditions	i) Ocean off until steady state; ice initially thin, thick, partially grounded	−1.9	N/A
	ii) Ocean off until steady state; ice initially thin, thick, partially grounded	−1.5	N/A
	iii) Ocean off until steady state; ice initially thin, thick, partially grounded	−1.25	Panels (a)–(b)
	iv) Ocean off until steady state; ice initially thin, thick, partially grounded	−1	Panels (c)–(d)
	ice initially thin, no bump		Panel c
	v) Ocean off until steady state; ice initially thin, thick, partially grounded	−0.75	N/A
Cavity shape	i) Alter shelf bottom after steady state; concave, convex	−1.25	N/A
	ii) alter shelf bottom after steady state; concave, convex	−1	N/A
	iii) Alter shelf bottom after steady state; concave, convex	−0.75	N/A
Initial conditions	i) Ocean–ice coupling throughout simulation; ice initially thin, thick, partially grounded	−1.25	Panels (a)–(b)
	ice initially partially grounded, 0.125 °C ocean cooling		Panel (a)
	ice initially partially grounded, no bump		Panel (a)
	ii) Ocean–ice coupling throughout simulation; ice initially thin, thick, partially grounded	−1	Panels (c)–(d)

shape. With a convex shelf bottom, peak melt magnitudes are focused near the ice front when compared to both the steady-state and more concave shelf cavities (Fig. 4). Therefore, in each of the forcing scenarios, deglaciation proceeds more rapidly with increasing concavity, such that grounding-line retreat across a given location is temporally offset by approximately 10–15 years, and, at a given time, is spatially offset by a few-to-ten kilometers.

3.3. Set three: Initial conditions with a coupled system

When the ice and ocean are coupled throughout the entire simulation (rather than spinning the ice up to an initial steady state without the ocean), feedbacks alter the evolution of the system so that the three initial ice profiles used in the first set of experiments no longer all lead to the same final steady state.

The thick, fully grounded initial condition retreats to the same steady-state position ($x_{gl}=81.1$ km) regardless of when the ocean is activated (dotted and solid red curves, Fig. 5a). Because its unforced tendency is to retreat monotonically and this retreat is only enhanced by ocean forcing, the ice stream thins throughout the simulation until it reaches a steady state. This removes the possibility of hysteretic behavior (Parizek et al., 2010).

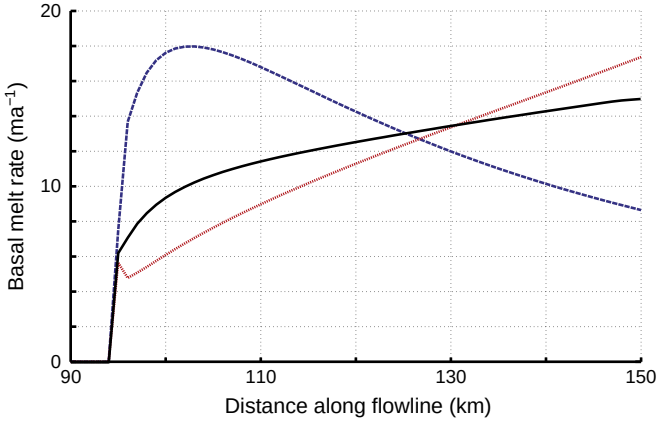

Fig. 4. Basal melt rates resulting from the initial steady-state (black), concave (dashed blue), and convex (dotted red) ice-shelf cavities (see Fig. 2b) at the onset of the −0.75 °C ocean-forcing scenario.

When the ice is initially grounded close to flotation with a $T_w(0)=-1.25$ °C ocean forcing, the "overshoot" that results from the system being so far out of balance is accentuated. Furthermore, there is no subsequent grounding-line advance because a new balance is reached farther inland between the grounding-line ice flux, the integrated basal melting rate over a longer ice shelf, and the free-radiation outflux (dashed black line in Fig. 5a–b). Therefore, the final grounding-line position ($x_{gl}=76.7$ km) does not match that resulting from the thicker, fully grounded initial profile ($x_{gl}=81.1$ km). The stabilizing effect of the bedrock bump removes this discrepancy under the warmer ocean scenario (Fig. 5c).

With a partially grounded initial condition, we find even greater differences in the final ice profiles. The grounding-line experiences a delayed advance to the sediment wedge in the colder ocean, but the ocean has too great of an influence to permit grounding of the ice along the entire leeward side. Therefore, the advance stalls at the bump (dashed blue in Fig. 5a–b). Notably, we find that a mere 0.125 °C cooling of the ambient ocean is sufficient to permit continued glaciation to the coupled steady-state position resulting from the previous experiments (solid blue in Fig. 5a). Furthermore, removal of the bedrock bump leads to a fourth equilibrium, with the advance stopping at $x_{gl}=74.0$ km (thin, dotted blue in Fig. 5a). It is important to note that, for the simulations under the $T_w(0)=-1.25$ °C ocean forcing with fully grounded initial conditions, the final grounding-line positions are unaffected by the presence/absence of the bump at 50 km. Therefore, three of the four steady states are a result of ocean–ice interactions and not the basal high. In a warmer ocean, the entire domain deglaciates (dashed blue, Fig. 5c,d) because melting at these depths exceeds the upstream ice flux. This is in stark contrast to the steady-state ice profile observed in Figure 3d under the same ambient ocean conditions.

In summary, with ice–ocean coupling throughout the duration of the runs, we find that both the transients and final grounding-line positions heavily depend on the initial and boundary conditions. In contrast, in the first set of experiments (ocean off → run to an initial steady state → ocean on → run to a final steady state), the final ice

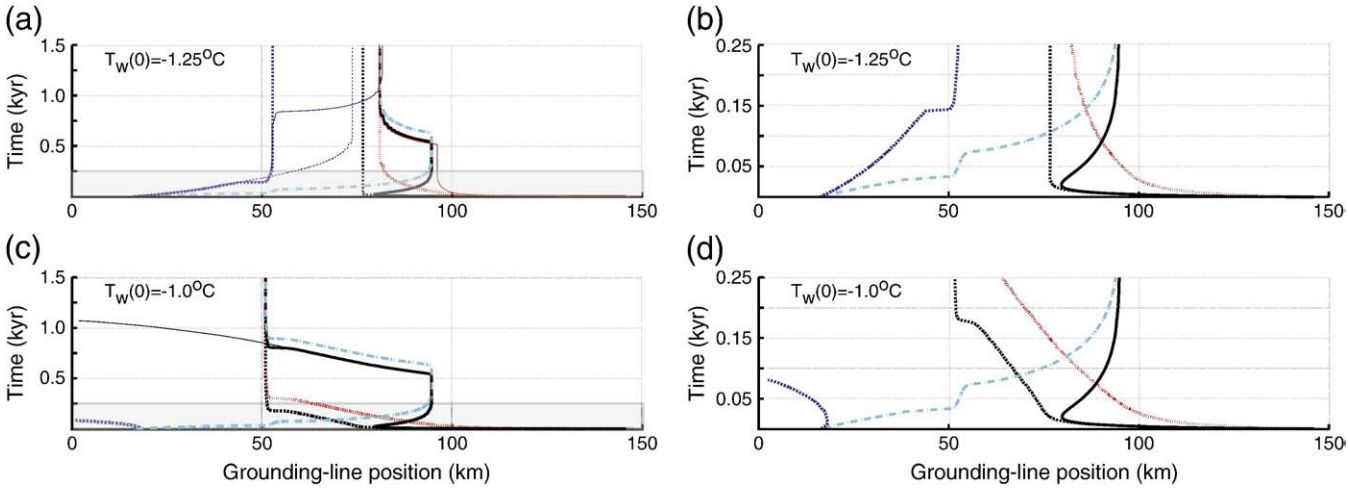

Fig. 5. Grounding-line histories for two different ocean-surface temperatures, (a)–(b) −1.25 °C and (c)–(d) −1.0 °C as in Figure 3c–d, respectively, and the various initial ice profiles in Figure 2a. Panels (b) and (d) highlight changes in the first 250 years. They include results shown within the boxed regions in (a) and (c), respectively, but with different scales on the ordinate axes. Recall that the bedrock bump is centered at 50 km. Black curves represent runs that start from the dashed black initial profile in Figure 2a with the ocean initially off (solid) and always on (dashed), respectively. See Table 2. The thin, dotted blue [thin, solid black] curve in (a) [(c)] results from the same forcing as the thicker dashed blue [black curve], however, the bump has been removed from the upsloping bed. Histories that start from the partially grounded blue profile in Figure 2a are also depicted with the ocean initially off (dot–dashed cyan) and always on (dashed blue). The solid blue curve in (a) is generated by the same initial ocean forcing as the dashed blue simulation, followed by a 0.125 °C ocean cooling. The dotted [solid] red curves result from starting with the dotted red profile in Figure 2a, with [initially without] ocean coupling.

profiles all coincide for a given ocean forcing, regardless of the initial conditions. Because the ocean is continually interacting with a marine ice sheet in the natural system, our results highlight the importance of both the forcing scenarios and the current history-dependent state of an ice sheet when predicting future system evolution. Vastly different outcomes can be realized under the same forcing.

4. Conclusions

Simulations of ice stream–ice shelf–ocean interactions in a setting where both the marine instability and the stabilizing effects of topographic highs are in play (e.g., along the Siple Coast in the Ross Embayment, Thwaites and Pine Island Glaciers in the Amundsen Sea Embayment) suggest that, for a given climate, grounding-line position is history-dependent. Therefore, the present state of an ice stream–ice shelf system, its overall catchment geometry and dynamics, and the ocean conditions into which it flows are extremely important in determining both the rate and magnitude of (de)glaciation, because different steady states are possible.

While water-mass conditions largely control the magnitude of melt along the base of an ice shelf, grounding-line motion is enhanced by a positive feedback between the ocean and ice. Focusing melt near the grounding-line leads to an increase in the local slope of the basal ice, thereby enhancing buoyancy-driven plume flow and subsequent melt rates. Therefore, the ambient water conditions and the initial geometry of the shelf bottom (convex/linear/concave) influence the melt rates and basal-melt distribution, thereby influencing the retreat history. Yet, inherent hysteresis in the system (arising due to non-linear dynamic feedbacks and the wide range of timescales involved) along with subtle geomorphic features at the bed can speed up, slow, or even temporarily reverse grounding-line migration (Alley et al., 2007; Anandakrishnan et al., 2007; Parizek et al., 2010).

Our modeling results continue to indicate that grounding lines become pinned on basal highs, such that we expect stasis, then jumps. Furthermore, advance and retreat dynamics in the vicinity of bedrock highs differ. Advance (retreat) towards the mound is accelerated by increased drag (the decreased rate of upstream thickening) and advance past the mound is slowed while the ice-shelf thickens to ground on the leeward side. In contrast, retreat past the mound is accelerated by enhancement of the marine instability. Taken together, grounding lines tend to have an affinity for bedrock highs.

The stabilizing effect of relatively minor topographic features is particularly noteworthy for informing future projections of ice-sheet contributions to sea-level rise, because the typical resolution of whole ice-sheet models that are currently used for such studies is too coarse to resolve these asperities. In addition, relative to the meters of sea-level change that are required to move a grounding line off of a bedrock high, minor perturbations $\mathcal{O}(0.1)$°C in ocean temperature can lead to grounding-line advance/retreat past a similar basal feature (Alley et al., 2007). This suggests that the relatively long-lived grounding-line stability observed along the Siple Coast could abruptly end with modest shifts in ocean circulation patterns. Therefore, coupling ice–ocean interactions with grounding zone dynamics and the interior ice-sheet reservoir is imperative for accurate assessments of future sea-level rise.

Acknowledgments

B.R. Parizek was supported by the U.S. National Science Foundation under grants 0531211, 0758274, 0909335, and the Center for Remote Sensing of Ice Sheets (CReSIS) 0424589 and by NASA under grants NRA-04-OES-02, NNX-09-AV94G, and NNX-10-AI04G. R.T. Walker was supported by NSF through grants 0909335 and CReSIS 0424589, by NASA under grants NNX-09-AV94G and NNX-10-AI04G, and by the Gary Comer Science and Education Foundation. We thank R.B. Alley for invaluable discussions and insights. Finally, we would like to recognize the efforts of the Editor, Peter deMenocal, and two anonymous referees. Their critical reviews significantly improved this manuscript.

References

Alley, R.B., Anandakrishnan, S., Dupont, T.K., Parizek, B.R., Pollard, D., 2007. Effect of sedimentation on ice-sheet grounding-line stability. Science 315, 1838–1841.
Anandakrishnan, S., Catania, G.A., Alley, R.B., Horgan, H.J., 2007. Discovery of till deposition at the grounding line of Whillans Ice Stream. Science 322, 1835–1838.
Budd, W.F., Jacka, T.H., 1989. A review of ice rheology for ice sheet modelling. Cold Reg. Sci. Technol. 16 (2), 107–144.
Drbohlav, J., Jin, F.F., 1998. Interdecadal variability in a zonally averaged ocean model: an adjustment oscillator. J. Phys. Oceanogr. 28, 1252–1270.

Dupont, T.K., 2009. Comparison of side stress and buttressing generated by flow-line and plan-view models of ice shelves, unpublished presentation made at the 2009 Midwest Glaciology Meeting, March 27–28, University of Chicago.
Dupont, T.K., Alley, R.B., 2005. Assessment of the importance of ice-shelf buttressing to ice-sheet flow. Geophys. Res. Lett. 32.
Dupont, T.K., Alley, R.B., 2006. Role of small ice shelves in sea-level rise. Geophys. Res. Lett. 33.
Durand, G., Gagliardini, O., de Fleurian, B., Zwinger, T., Le Meur, E., 2009. Marine ice sheet dynamics: hysteresis and neutral equilibrium. J. Geophys. Res. 114.
Fricker, H.A., Coleman, R., Padman, L., Scambos, T.A., Bohlander, J., Brunt, K.M., 2009. Mapping the grounding zone of the Amery Ice Shelf, East Antarctica using InSAR, MODIS and ICESat. Antarct. Sci. 21 (5), 515–532.
Glen, J.W., 1955. The creep of polycrystalline ice. Proceedings of the Royal Society., Vol. 228 of A, pp. 519–538.
Goldberg, D., Holland, D.M., Schoof, C., 2009. Grounding line movement and ice shelf buttressing in marine ice sheets. J. Geophys. Res. 114.
Holland, D.M., Jenkins, A., 1999. Modeling thermodynamic ice–ocean interactions at the base of an ice shelf. J. Phys. Oceanogr. 29, 1787–1800.
Holland, D.M., Thomas, R.H., D., B., Ribergaard, M.H., Lyberth, B., 2008. Acceleration of jakobshavn isbr triggered by warm subsurface ocean waters. Nat. Geosci. 1, 659–664.
Holt, J.W., Blankenship, D.D., Morse, D.L., Young, D.A., Peters, M.E., Kempf, S.D., Richter, T.G., Vaughan, D.G., Corr, H.F.J., 2006. New boundary conditions for the West Antarctic ice sheet: subglacial topography of the Thwaites and Smith glacier catchments. Geophys. Res. Lett. 33.
Horgan, H.J., Anandakrishnan, S., 2006. Static grounding lines and dynamic ice streams: evidence from the Siple Coast, West Antarctica. Geophys. Res. Lett. 33.
Howat, I.M., Joughin, I., Tulaczyk, S., Gogineni, S., 2005. Rapid retreat and acceleration of Helheim Glacier, east Greenland. Geophys. Res. Lett. 32.
Hulbe, C.L., MacAyeal, D.R., Denton, G.H., Kleman, J., Lowell, T.V., 2004. Catastrophic ice shelf breakup as the source of Heinrich event icebergs. Paleoceanography 19.
Jenkins, A., 1991. A one-dimensional model of ice shelf-ocean interaction. J. Geophys. Res. 96 (C11), 20671–20677.
Joughin, I., Abdalati, W., Fahnestock, M., 2004. Large fluctuations in speed on Greenland's Jakobshavn Isbrae glacier. Nature 432, 608–610.
Little, C.M., Gnanadesikan, A., Oppenheimer, M., 2009. How ice shelf morphology controls basal melting. J. Geophys. Res. 114.
MacAyeal, D.R., 1989. Large-scale ice flow over a viscous basal sediment: theory and application to Ice Stream B, Antarctica. J. Geophys. Res. 94 (B4), 4071–4087.
Parizek, B.R., Alley, R.B., 2004. Implications of increased Greenland surface melt under global-warming scenarios: ice-sheet simulations. Quatern. Sci. Rev. 23, 1013–1027.
Parizek, B.R., Alley, R.B., Dupont, T.K., Walker, R.T., Anandakrishnan, S., 2010. Effect of orbital-scale climate cycling and meltwater drainage on ice sheet grounding line migration. J. Geophys. Res. 115 (F01011). doi:10.1029/2009JF001325.
Pattyn, F., 2002. Transient glacier response with a higher-order numerical ice-flow model. J. Glaciol. 48 (162), 467–477.
Pattyn, F., Huyghe, A., De Brabander, S., De Smedt, B., 2006. Role of transition zones in marine ice sheet dynamics. J. Geophys. Res. 111.
Payne, A.J., Vieli, A., Shepherd, A.P., Wingham, D.J., Rignot, E., 2004. Recent dramatic thinning of largest West Antarctic ice stream triggered by oceans. Geophys. Res. Lett. 31.
Payne, A.J., Holland, P.R., Shepherd, A.P., Rutt, I.C., Jenkins, A., Joughin, I., 2007. Numerical modeling of ocean–ice interactions under Pine Island Bay's ice shelf. J. Geophys. Res. 112.
Rignot, E., Bamber, J.L., van den Broeke, M.R., Davis, C., Li, Y., van de Berg, W.J., van Meijgaard, E., 2008a. Recent Antarctic ice mass loss from radar interferometry and regional climate modelling. Nat. Geosci. 1.
Rignot, E., Box, J.E., Burgess, E., Hanna, E., 2008b. Mass balance of the Greenland ice sheet from 1958 to 2007. Geophys. Res. Lett. 35.
Scambos, T.A., Hulbe, C., Fahnestock, M., Bohlander, J., 2000. The link between climate warming and break-up of ice shelves in the Antarctic Peninsula. J. Glaciol. 46 (154), 516–530.
Scambos, T.A., Hulbe, C., Fahnestock, M., 2003. Climate-induced ice shelf disintegration in the Antarctic Peninsula. In: et al., E.D. (Ed.), Antarctic Peninsula Climate Variability: Historical and Paleoenvironmental Perspectives, Antarct. Res. Ser. AGU, Washington, D.C., p. 79 92.
Scambos, T.A., Bohlander, J.A., Shuman, C.A., Skvarca, P., 2004. Glacier acceleration and thinning after ice shelf collapse in the Larsen B embayment, Antarctica. Geophys. Res. Lett. 31.
Schoof, C., 2007a. Ice sheet grounding line dynamics: steady states, stability, and hysteresis. J. Geophys. Res. 112, F3.
Schoof, C., 2007b. Marine ice sheet dynamics. Part I. The case of rapid sliding. J. Fluid Mech. 573, 27–55.
Sergienko, O., MacAyeal, D.R., 2005. Surface melting on Larsen ice shelf. Antarct. Ann. Glaciol. 40, 215–218.
Solomon, S., Qin, D., Manning, M., Chen, Z., Marquis, M., Averyt, K.B., Tignor, M., Miller, H.L. (Eds.), 2007. Climate Change 2007: The Physical Science Basis. Contribution of Working Group I to the Fourth Assessment Report of the Intergovernmental Panel on Climate Change. Cambridge University Press, Cambridge, United Kingdom and New York, NY, USA.
Stigebrandt, A., 1987. A model for the vertical circulation of the Baltic Deep Water. J. Phys. Oceanogr. 17, 1772–1785.
Thomas, R.H., 1977. Calving bay dynamics and ice-sheet retreat up the St. Lawrence Valley System. Geogr. Phys. Quat. 31, 347–356.
Thomas, R.H., Bentley, C.R., 1978. A model for Holocene retreat of the West Antarctic ice sheet. Quatern. Res. 10, 150–170.
Thomas, R., Rignot, E., Casassa, G., Kanagaratnam, P., Acuna, C., Akins, T., Brecher, H., Frederick, E., Gogineni, P., Krabill, W., Manizade, S., Ramamoorthy, H., A, A.R., Russell, R., Sonntag, J., Swift, R., Yungel, J., Zwally, J., 2004. Accelerated sea-level rise from West Antarctica. Science 306, 255–258.
Van den Broeke, M., 2005. Strong surface melting preceded collapse of Antarctic Peninsula ice shelf. Geophys. Res. Lett. 32.
Vieli, A., Payne, A.J., 2005. Assessing the ability of numerical ice sheet models to simulate grounding line migration. J. Geophys. Res. Earth Surf. 110.
Walker, R.T., Holland, D.M., 2007. A two-dimensional coupled model for ice shelf-ocean interaction. Ocean Modell. 17, 123–139.
Walker, R.T., Dupont, T.K., Parizek, B.R., Alley, R.B., 2008. Effects of basal-melting distribution on the retreat of ice-shelf grounding lines. Geophys. Res. Lett. 35.
Weertman, J., 1974. Stability of the junction of an ice sheet and an ice shelf. J. Glaciol. 13 (67), 3–11.
Wright, D.G., Stocker, T.F., 1991. A zonally averaged ocean model for the thermohaline circulation. Part I: model development and flow dynamics. J. Phys. Oceanogr. 21, 1713–1724.